PCCP

PAPER

View Article Online
View Journal | View Issue

Cite this: *Phys. Chem. Chem. Phys.*, 2018, **20**, 12710

^{209}Bi quadrupole relaxation enhancement in solids as a step towards new contrast mechanisms in magnetic resonance imaging

D. Kruk, *[a] E. Umut,[a] E. Masiewicz,[a] C. Sampl,[b] R. Fischer,[b] S. Spirk,[b] C. Goesweiner[c] and H. Scharfetter[c]

Received 11th February 2018,
Accepted 19th March 2018

DOI: 10.1039/c8cp00993g

rsc.li/pccp

Motivated by the possibility of exploiting species containing high spin quantum number nuclei (referred to as quadrupole nuclei) as novel contrast agents for Magnetic Resonance Imaging, based on Quadrupole Relaxation Enhancement (QRE) effects, ^{1}H spin–lattice relaxation has been investigated for tris(2-methoxyphenyl)bismuthane and tris(2,6-dimethoxyphenyl)bismuthane in powder. The relaxation experiment has been performed in the magnetic field range of 0.5 T to 3 T (the upper limit corresponds to the field used in many medical scanners). A very rich QRE pattern (several frequency specific ^{1}H spin–lattice relaxation rate maxima) has been observed for both compounds. Complementary Nuclear Quadrupole Resonance experiments have been performed in order to determine the quadrupole parameters (quadrupole coupling constant and asymmetry parameters) for ^{209}Bi. Knowing the parameters, the QRE pattern has been explained on the basis of a quantum-mechanical picture of the system including single and double-quantum coherences for the participating nuclei (^{1}H and ^{209}Bi). In this way the quantum-mechanical origin of the spin transitions leading to the QRE effects has been explained.

1. Introduction

Magnetic Resonance Imaging (MRI) is one of the most versatile and powerful diagnostic tools due to its superior intrinsic soft tissue contrast. MRI provides spatially and temporally resolved maps of ^{1}H relaxation times of the inside of human bodies. The observation that ^{1}H relaxation times of healthy tissues and tumours differ was made decades ago.[1,2] This discovery has motivated the scientific community to extensive studies on how to exploit this effect by enlarging the difference (contrast) in the relaxation times between healthy and pathological tissues. The studies have given rise to a development of paramagnetic contrast agents causing Paramagnetic Relaxation Enhancement (PRE) effects.[3–5] Paramagnetic contrast agents are complexes of transition or rare-earth metal ions; in clinical practice usually gadolinium (Gd) based chelates are used.[3,5] Very strong magnetic electron–proton dipole–dipole interactions between the electron spin of the paramagnetic species and neighbouring proton spins lead to very fast proton spin relaxation (the relaxation rates become larger – in other words, the relaxation is enhanced). Taking into account the ratio between the electron and proton gyromagnetic factors ($\approx$659), the large spin of Gd ions (S = 7/2) and the fact that the ^{1}H relaxation rate depends on a square of the electron gyromagnetic factor one could expect a very large enhancement of the relaxation rate. The observed ^{1}H paramagnetic relaxation enhancement is, however, much smaller. The reason of that is electron spin relaxation that acts as an additional (besides the molecular motion) source of modulations of the electron–proton dipole–dipole interaction.[3,4,6–9] The electron spin relaxation is independent of the presence of neighbouring protons as its predominating mechanism is Zero Field Splitting (ZFS) interactions. The ZFS coupling is so strong that it leads to very fast electron spin relaxation and, in consequence, the ^{1}H relaxation enhancement is far below the expected value.[3,4,6] The relaxation enhancement observed for typical paramagnetic contrast agents is by the factor of 20–50 larger[10,11] compared to ^{1}H relaxation in water (referring to 1 mmol concentration of the paramagnetic species). The PRE effects have been a subject of extensive theoretical studies motivated not only by the diagnostic applications, but also as a very interesting and demanding problem of quantum-mechanical theory of spin relaxation. The theory of PRE has started from very simple models,[3,8,12,13] developing towards advanced, comprehensive theoretical tools predicting PRE values for arbitrary magnetic field, interaction strengths and motional conditions.[3–5,8,9,14–16]

[a] *University of Warmia & Mazury in Olsztyn, Faculty of Mathematics and Computer Science, Słoneczna 54, PL-10-710 Olsztyn, Poland.*
E-mail: danuta.kruk@matman.uwm.edu.pl; Tel: +48 89 524 60 11
[b] *Institute for Chemistry and Technology of Materials, Graz University of Technology, Stremayrgasse 9, 8010 Graz, Austria*
[c] *Institute of Medical Engineering, Graz University of Technology, Stremayrgasse 16/III, A-8010 Graz, Austria*

These theoretical tools are very useful for tailoring properties of paramagnetic contrast agents to obtain the desired enhancement effects. As far as paramagnetic contrast agents are concerned, significant effort has also gone into the development of nanoparticles containing iron oxides.[17,18] In the last few years, the concept of "smart" paramagnetic contrast agents that not only lead to the relaxation enhancement, but additionally exhibit on and off switches or are sensitive to physiological parameters such as pH has been developed.[11,19] This comprehensive effort directed towards exploiting the potential of paramagnetic contrast agents has significantly contributed to make MRI the key method of non-invasive medical diagnostics.

Nuclear Magnetic Resonance (NMR) methods are widely used not only in medicine, but also in generally understood molecular science to investigate dynamics and structure of condensed matter. A special role plays NMR relaxometry. "Classical" relaxation experiments are performed at a single, relatively high magnetic field (resonance frequency) *versus* temperature. In NMR relaxometry experiments the magnetic field and hence the resonance frequency varies in a broad range so one can measure spin–lattice relaxation rate *versus* the resonance frequency. In this way ^{1}H spin–lattice quadrupole relaxation enhancement (QRE) has been discovered in biological systems[20–25] and various solids containing ^{14}N nuclei.[26,27] ^{14}N nuclei possess spin $S = 1$ and therefore, when placed in an electric field gradient (EFG), exhibit quadrupole interaction. The principles of the QRE effect is as follows. The ^{1}H and the quadrupole nucleus (a nucleus possessing a quadrupole moment) are coupled by a magnetic dipole–dipole interaction. As a result of its Zeeman interaction the ^{1}H nucleus ($I = 1/2$) can occupy two states described by the magnetic quantum numbers $m_I = \pm 1/2$. At the same time the energy level structure of the quadrupole nucleus stems from a superposition of its quadrupole and Zeeman couplings; in fact, except of high magnetic fields, it is dominated by the quadrupole coupling that does not depend of the magnetic field. Thus, there are magnetic fields at which the ^{1}H energy level splitting matches one of the transitions of the quadrupole nucleus between its energy levels. When the dynamics of the system is slow (like in solids) at these magnetic fields (^{1}H frequencies) the ^{1}H magnetisation can be transferred to the quadrupole nucleus; this manifests itself as a faster ^{1}H decay – *i.e.* a frequency specific ^{1}H spin–lattice relaxation enhancement (quadrupole peaks).[20–28] For ^{14}N one observes three relaxation maxima.[20–30] As far as higher spin quantum number quadrupole nuclei are concerned, there are some indications of the QRE effects in LaF_3.[31,32]

In this context the question arises whether QRE can be exploited as a mechanism for novel extrinsic MRI contrast agents. The essential difference between the PRE and QRE effects is that in the first case a ^{1}H relaxation enhancement is observed in the whole frequency range as a result of a strong proton–electron dipole–dipole coupling. In the case of QRE the relaxation enhancement appears only at selected frequencies – therefore it can be switched on and off in response to subtle changes in the EFG. This opens the possibility for designing smart contrast agents for molecular imaging which change contrast *e.g.* by chemical interaction with the surrounding tissues. One could argue that the QRE effects are too weak to be exploited as a contrast mechanism. To increase the contrast one has to use high spin quantum number nuclei of $S = 9/2$ or $S = 7/2$, but this is obviously not sufficient – the electronic spin of Gd^{3+} is also 7/2. However, due to very fast electron spin relaxation which leads to a reduction of ^{1}H spin–lattice relaxation[3,4,6–11] the PRE enhancement is much lower than one could expect from the large electronic gyromagnetic factor. The quadrupole spin relaxation is slow and this acts towards increasing ^{1}H spin–lattice relaxation rate.

Among several high spin quadrupole nuclei we consider ^{209}Bi as a very promising candidate because of its large quadrupole moment that opens the opportunity to observe QRE effects at high magnetic field (3 T) used in many clinical MRI scanners and because of its comparatively low toxicity. To explore the potential of ^{209}Bi compounds as possible contrast agents it is necessary to reveal details of the quantum-mechanical mechanism of QRE for $S = 9/2$. For this purpose two ^{209}Bi compounds have been chosen: tris(2-methoxyphenyl)bismuthane ($C_{21}H_{21}BiO_3$) and tris(2,6-dimethoxyphenyl)bismuthane ($C_{24}H_{27}BiO_6$). ^{1}H spin–lattice relaxation experiments have been performed for the system revealing a rich QRE pattern; to our knowledge this is the first experimental observation of QRE effects for high spin quadrupole nuclei (the examples reported in literature concern ^{14}N). The QRE pattern has been associated with specific spin transitions and thoroughly discussed.

The paper is organized as follows: in Section 2 the principles of QRE are presented, Section 3 contains experimental details, in Section 4 the data are presented and discussed, while Section 5 includes concluding remarks.

2. Quadrupole interactions and relaxation enhancement effects

As already explained, the term QRE refers to frequency specific ^{1}H spin–lattice relaxation maxima resulting from a magnetic dipole–dipole coupling between ^{1}H and a high spin nucleus ($S > 1/2$), ^{209}Bi ($S = 9/2$) in this case. QRE is a complex quantum-mechanical phenomenon;[25,28] here we shall outline its basic concept. The high spin nucleus placed in an electric field gradient (EFG) exhibits a quadrupole coupling (therefore we shall call it "quadrupole nucleus"). The energy level structure of the quadrupole nucleus is determined by a sum of its Zeeman, $H_Z(S)$, and quadrupole, $H_Q(S)$, Hamiltonians, denoted as $H_0(S)$:[33]

$$H_0(S) = H_Z(S) + H_Q(S)(\Omega)$$
$$= \omega_S S_z + \frac{1}{2}\sqrt{\frac{3}{2S(2S-1)}}\, a_Q \sum_{m=-2}^{2} (-1)^m F^2_{-m}(\Omega) T^2_m,$$

$\omega_S = \gamma_S B_0$ is its resonance frequency, while $aQ = e^2qQ/\hbar$ denotes the quadrupole coupling constant, with γ_S: gyromagnetic factor, B_0: magnetic flux density, Q: quadrupole moment of the nucleus and q is the zz component of the

electric field gradient tensor. The tensor operators are defined as: $T^2_0(S)=\frac{1}{\sqrt{6}}\left[3S_z^2-S(S+1)\right]$, $T^2_{\pm1}(S)=\mp\frac{1}{2}[S_zS_\pm+S_\pm S_z]$ and $T^2_{\pm2}(S)=\frac{1}{2}S_\pm S_\pm$, while the spatial components of the quadrupole Hamiltonian are given as: $F^2_{-m}(\Omega)=D^2_{0,-m}(\Omega)+\frac{\eta}{\sqrt{6}}\left[D^2_{2,-m}(\Omega)+D^2_{-2,-m}(\Omega)\right]$, where η is the asymmetry parameter of the EFG tensor, $D^2_{k,\ -m}(\Omega)$ denotes the Wigner rotation matrices.[34,35] The angle Ω describes the orientation of the principal axis system of the EFG with respect to the direction of the external magnetic field (laboratory frame). This implies that energy levels of the quadrupole nucleus depend on the orientation. They can be obtained by diagonalizing the matrix representation of the Hamiltonian $H_0(S)$ in the basis $\{|S,m_S\rangle\}$ (m_S denotes magnetic quantum numbers) that leads to a set of eigenfunctions $\{|\psi_\alpha(\Omega)\rangle\}$ of the S spin which are linear combinations of the functions $|n\rangle = |S,m_S\rangle$: $|\psi_\alpha(\Omega)\rangle=\sum_{n=1}^{2S+1}a_{\alpha n}(\Omega)|n\rangle$, and a set of corresponding eigenvalues (energy levels). This implies that the $|n\rangle = |S,m_S\rangle$ vectors are not the eigenvectors of the quadrupole nucleus. The basis $\{|S,m_S\rangle\}$ (referred to as Zeeman basis) is the eigenbasis only in the high field range, when the Zeeman interaction is much stronger than the quadrupole coupling or when $\Omega = 0$ and $\eta = 0$. In a general case each eigenvector $|\psi_\alpha\rangle$ includes vectors $|S,m_S\rangle$ of different magnetic spin quantum numbers, m_S. Dipole–dipole interactions between ^{1}H and the quadrupole nucleus are the source of ^{1}H relaxation. This means that the transition of ^{1}H between its energy levels is coupled to the transitions of the quadrupole nucleus – in this way ^{1}H "feels" the energy level structure of the quadrupole nucleus. When the ^{1}H resonance frequency, ω, matches one of the transition frequencies $\omega_{\alpha\beta} = \omega_\alpha - \omega_\beta$ (ω_α,ω_β denote energy levels corresponding to eigenvectors $|\psi_\alpha\rangle$ and $|\psi_\beta\rangle$, respectively) of the S-spin nucleus, the ^{1}H magnetisation can be transferred to the quadrupole nucleus, thus leading to a faster decay of the ^{1}H magnetisation – *i.e.* an enhancement of ^{1}H spin–lattice relaxation, referred to as the QRE. This process can involve two protons coupled by a dipolar interaction (provided the coupling is not fully averaged out by molecular motion).[28–30] In this case QRE effects can also occur when the frequency of the joint (double-quantum) transition of two coupled ^{1}H nuclei, 2ω, matches one of the $\omega_{\alpha\beta}$ frequencies.

The explicit form of the Hamiltonian $H_0(S)$ in the basis $\{|S,m_S\rangle\}$ is given in Appendix.

3. Materials and methods

^{1}H NMR spin–lattice relaxation experiments were performed for tris(2-methoxyphenyl)bismuthane ($C_{21}H_{21}BiO_3$) and tris(2,6-dimethoxyphenyl)bismuthane ($C_{24}H_{27}BiO_6$) in powder form. The structure of the compounds is shown in Fig. 1. The experiment was performed at 295 K (temperature stability 1 K) in the frequency range of 20 MHz–128 MHz using superconducting magnet operating up to magnetic field of 3 T compatible with STELAR Spinmaster Fast Field Cycling (FFC) relaxometer.

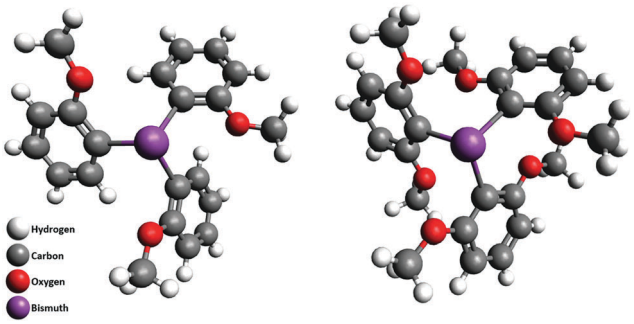

Fig. 1 Structure of tris(2-methoxyphenyl)bismuthane (left) and tris(2,6-dimethoxyphenyl)bismuthane (right).

The measurements were performed with an inversion-recovery pulse sequence with the 90° pulse length between 3.5–5.0 μs. It turned out that the magnetisation evolution is, in a good approximation, single exponential in the whole frequency range; examples are shown in Fig. 2.

NQR-data were collected using two complementary pulse type NQR spectrometers equipped with gas (air)-flow thermal control system for 10 °C up to 50 °C. First the unknown NQR peaks were located by fast explorative scans with the custom-built spectrometer "Graz-NQRS-MK1"[36] over wide bands up to 50 MHz Then the NQR parameters and peak shapes were determined with the commercially available "Scout" (Tecmag, Inc., USA), which allows advanced pulse sequence programming including phase cycling. Both spectrometers are driven by a 500 W power amplifier that can supply a set of different solenoid RF-coils of 10 mm diameter all together covering a range of 20 MHz up to 150 MHz. Usually spin echo (SE) and free induction decay (FID) rectangular pulse sequences were used to address the samples of solid, crystalline powders, filled in glass vials of 10 mm diameter and 40 mm length. The NQR measurements were performed at 310 K.

4. Results and analysis

The NQR experiments have revealed four ^{209}Bi spectral lines for tris(2-methoxyphenyl)bismuthane at the frequencies of 29.82 MHz, 59.64 MHz, 89.47 MHz and 119.27 MHz. The quadrupole constant, a_Q, and the asymmetry parameter, η of the ^{209}Bi were determined by diagonalization of the quadrupole spin Hamiltonian, $H_Q(S)$ for $\Omega = 0$ which gives the ^{209}Bi energy levels and hence the transition frequencies as a function of a_Q and η. As the experiment was performed at zero magnetic field the Zeeman Hamiltonian, $H_Z(S)$ needs not be considered and there is no need to discuss relative orientations of the principal axis system of the quadrupole interaction and the direction of the external magnetic field, (moreover, eigenvalues of a Hamiltonian do not depend of a reference frame). The positions of the NQR lines can be well reproduced for $a_Q = 715.3 \pm 0.4$ MHz and $\eta = 0 \pm 0.001$. This is the limiting case when the Zeeman basis $\{|S,m_S\rangle\}$ is the eigenbasis of the quadrupole nucleus. In consequence, one can talk about single-quantum spin transitions – *i.e.* transitions between energy levels associated with $|S,m_S\rangle$ and $|S,m_S'\rangle$ vectors

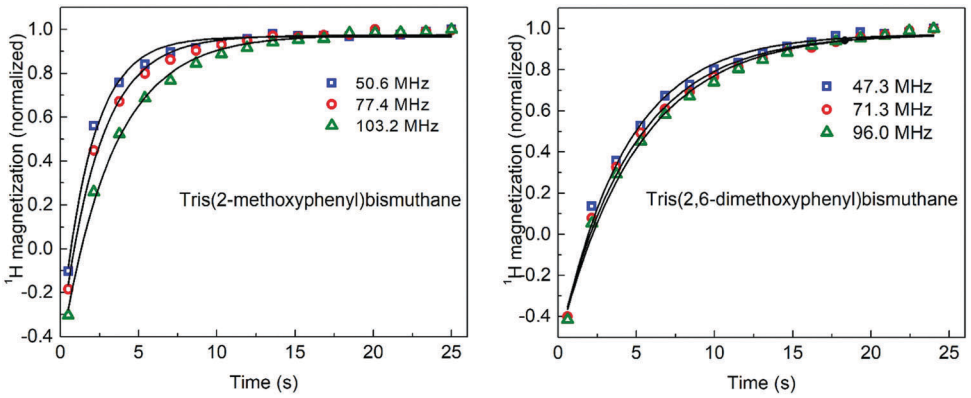

Fig. 2 ^{1}H magnetisation *versus* time for tris(2-methoxyphenyl)bismuthane (left) and tris(2,6-dimethoxyphenyl)bismuthane (right); solid lines – single exponential fits.

for which $|m_S - m_S'| = 1$. The single-quantum ^{209}Bi transitions correspond to the above frequencies of 29.82 MHz, 59.61 MHz, 89.41 MHz and 119.21 MHz that are associated with the following changes of the magnetic spin quantum number m_S: 3/2 → 1/2, 5/2 → 3/2, 7/2 → 5/2 and 9/2 → 7/2, respectively. For tris(2,6-dimethoxyphenyl)bismuthane the three NQR lines recorded at the frequencies 54.40 MHz, 82.45 MHz and 110.06 MHz give a_Q = 660.9 ± 0.4 MHz and η = 0.105 ± 0.001. As in this case $\eta \neq 0$ the eigenvectors of the quadrupole Hamiltonian are not represented by a single $|S,m_S\rangle$ vector, but by their linear combinations. In consequence, one cannot attribute these frequencies to the "pure" 7/2 → 5/2 and 9/2 → 7/2 transitions.

The ^{1}H spin–lattice relaxation data (relaxation rate, R_1, *versus* the resonance frequency) for tris(2-methoxyphenyl)bismuthane and tris(2,6-dimethoxyphenyl)bismuthane are shown in Fig. 3(a) and (b), respectively. One can see several relaxation maxima (QRE peaks). As explained in Section 2, ^{1}H spin–lattice QRE maxima can appear at ^{1}H frequencies matching one of the ^{209}Bi transitions between its energy levels which depend on the orientation of the principal axis system of the quadrupole coupling with respect to the direction of the external magnetic field. Fig. 4(a) and (b) show the energy levels for Ω = 0 and a_Q = 715.27 MHz, η = 0 (tris(2-methoxyphenyl)bismuthane) and a_Q = 660.94 MHz, η = 0.105 (tris(2,6-dimethoxyphenyl)bismuthane), respectively. As already explained, in the first case (η = 0), the $|S,m_S\rangle$ functions are the eigenvectors of the total Hamiltonian: $H_0(S) = H_Q(S) + H_Z(S)$; therefore the energy levels in Fig. 4(a) have been attributed to the $|S,m_S\rangle$ eigenvectors. This does not apply to $\Omega \neq 0$; then the eigenvectors are given as linear combinations of the $|S,m_S\rangle$. In the second case when $\eta \neq 0$ (tris(2,6-dimethoxyphenyl)bismuthane), even for Ω = 0 [Fig. 4(b)] the $|S,m_S\rangle$ vectors are not eigenvectors of the *S*-spin. Nevertheless we have kept the same colour scheme in Fig. 4(b) as in Fig. 4(a) taking as a reference the $|S,m_S\rangle$ vector to which the eigenvector $|\psi_\alpha\rangle$ converges in the high field limit.

For the purpose of the further discussion it is useful to introduce the following nomenclature: a transition between the energy levels associated with the eigenvectors $|\psi_i\rangle$ and $|\psi_j\rangle$ that in the high field range converge to the vectors $|S,m_S\rangle$ and $|S,m_S'\rangle$, respectively, will be denoted as $|\psi_i\rangle \rightarrow |\psi_j\rangle$ (m_S, m_S').

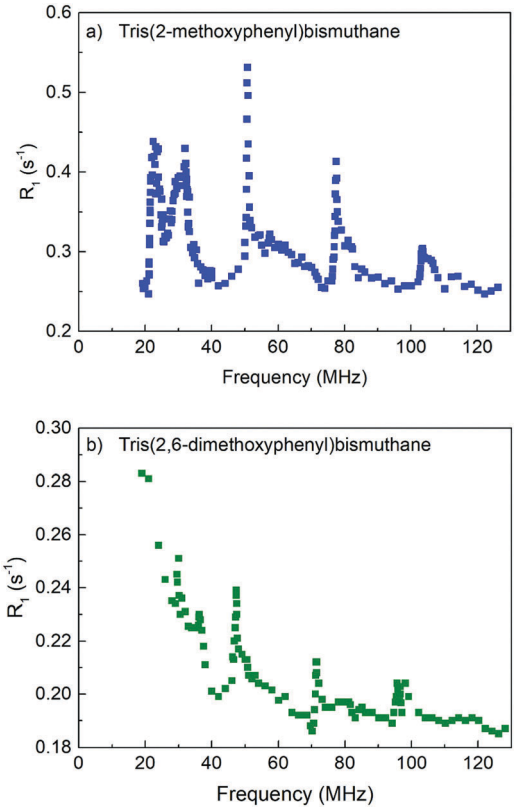

Fig. 3 ^{1}H spin–lattice relaxation rate *versus* frequency for (a) tris-(2-methoxyphenyl)bismuthane and (b) tris(2,6-dimethoxyphenyl)bismuthane.

It is very important to remember that, except of the high field limit, the $|\psi_i\rangle$ eigenvectors include a combination of $|S,m_S\rangle$ vectors of different m_S values.

To attribute the positions of the ^{1}H spin–lattice relaxation maxima to specific ^{209}Bi transitions it is necessary to thoroughly analyse the orientation dependence of the energy level structure. In Fig. 5(a) ^{209}Bi transition frequencies $|\psi_i\rangle \rightarrow |\psi_j\rangle$ (m_S, $m_S - 1$) are plotted *versus* ^{1}H resonance frequency, covering all orientations Ω. The areas representing the transition frequencies for the whole Ω range are crossed by a line representing the ^{1}H resonance frequency, corresponding to the ^{1}H transition

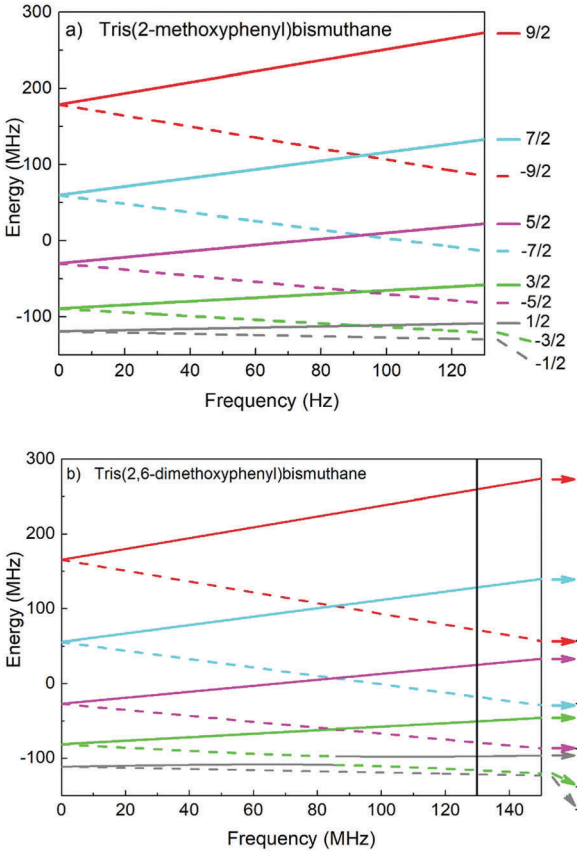

Fig. 4 ^{209}Bi energy levels *versus* magnetic field converted to ^{1}H resonance frequency for Ω = 0 calculated for (a) tris(2-methoxyphenyl)bismuthane (a_Q = 715.27 MHz, η = 0) and (b) tris(2,6-dimethoxyphenyl)bismuthane (a_Q = 660.94 MHz, η = 0.105).

between the energy levels described by the magnetic quantum numbers m_I = 1/2 and m_I = −1/2. One can see from Fig. 5(a) (top) that the $|\psi_\mu\rangle \rightarrow |\psi_\mu'\rangle$ (1/2, −1/2) transition frequency of ^{209}Bi (grey) is smaller than the ^{1}H resonance frequency. Thus, we are left with four ^{209}Bi transitions: $|\psi_\alpha\rangle \rightarrow |\psi_\alpha'\rangle$ (3/2, 1/2), $|\psi_\beta\rangle \rightarrow |\psi_\beta'\rangle$ (5/2, 3/2), $|\psi_\gamma\rangle \rightarrow |\psi_\gamma'\rangle$ (7/2, 5/2) and $|\psi_\delta\rangle \rightarrow |\psi_\delta'\rangle$ (9/2, 7/2), frequencies of which are projected onto the ^{1}H spin–lattice relaxation data for tris(2-methoxyphenyl)bismuthane [Fig. 5(a), bottom]. The data show five QRE peaks referred to as I, II, III, IV and V. One can see that the position of the low frequency peak (I) cannot be explained as a result of $|\psi_i\rangle \rightarrow |\psi_j\rangle$ (m_S, m_S − 1) transitions. QRE peaks denoted as II and III are associated with the $|\psi_\alpha\rangle \rightarrow |\psi_\alpha'\rangle$ (3/2, 1/2) and $|\psi_\beta\rangle \rightarrow |\psi_\beta'\rangle$ (5/2, 3/2) ^{209}Bi transitions, respectively. The QRE peak IV again cannot be explained by one of the $|\psi_i\rangle \rightarrow |\psi_j\rangle$ (m_S, m_S − 1) transitions, while peak V is associated with the $|\psi_\gamma\rangle \rightarrow |\psi_\gamma'\rangle$ (7/2, 5/2) ^{209}Bi transition. In the frequency range covered in this experiment one does not observe a QRE peak being a consequence of the $|\psi_\delta\rangle \rightarrow |\psi_\delta'\rangle$ (9/2, 7/2) ^{209}Bi transition, but its existence is not excluded – the effect might possibly appear above 130 MHz. Thus, summarizing, three ^{1}H spin–lattice relaxation maxima observed for tris(2-methoxyphenyl)bismuthane can be attributed to the $|\psi_\alpha\rangle \rightarrow |\psi_\alpha'\rangle$ (3/2, 1/2), $|\psi_\beta\rangle \rightarrow |\psi_\beta'\rangle$ (5/2, 3/2) and $|\psi_\gamma\rangle \rightarrow |\psi_\gamma'\rangle$ (7/2, 5/2) ^{209}Bi transitions combined with

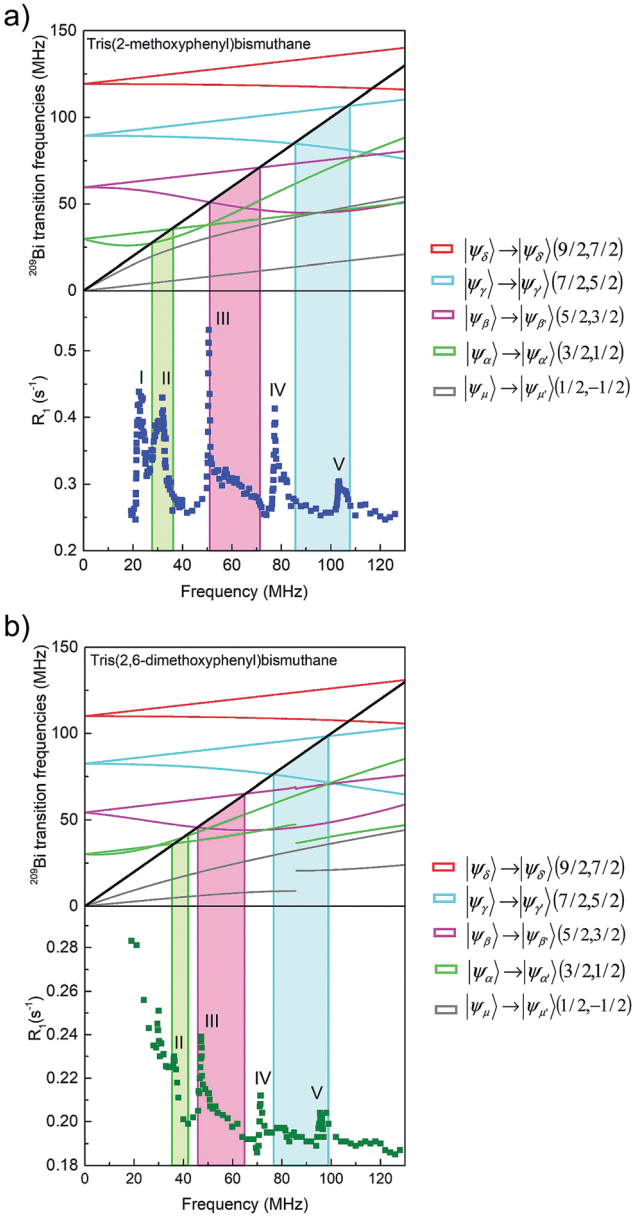

Fig. 5 (a) ^{209}Bi transition frequencies $|\psi_i\rangle \rightarrow |\psi_j\rangle$ (m_S, m_S − 1) in tris-(2-methoxyphenyl)bismuthane and ^{1}H resonance frequency (corresponding to ^{1}H single quantum transition) taking into account all orientations of the principal axis system of the electric field gradient with respect to the external magnetic field (whole range of Ω angle) compared with the experimental ^{1}H spin–lattice relaxation data. The ranges in which the transition frequencies $|\psi_\alpha\rangle \rightarrow |\psi_\alpha'\rangle$ (3/2, 1/2), $|\psi_\beta\rangle \rightarrow |\psi_\beta'\rangle$ (5/2, 3/2) and $|\psi_\beta\rangle \rightarrow |\psi_\beta'\rangle$ (7/2, 5/2) match the ^{1}H resonance frequency correspond to the positions of ^{1}H relaxation maxima denoted as II, III and V, respectively. (b) ^{209}Bi transition frequencies $|\psi_i\rangle \rightarrow |\psi_j\rangle$ (m_S, m_S − 1) in tris(2,6-dimethoxyphenyl)bismuthane and ^{1}H resonance frequency (corresponding to ^{1}H single quantum transition) taking into account all orientations of the principal axis system of the electric field gradient with respect to the external magnetic field (whole range of Ω angle) compared with the experimental ^{1}H spin–lattice relaxation data. The ranges in which the transition frequencies $|\psi_\alpha\rangle \rightarrow |\psi_\alpha'\rangle$ (3/2, 1/2), $|\psi_\beta\rangle \rightarrow |\psi_\beta'\rangle$ (5/2, 3/2) and $|\psi_\beta\rangle \rightarrow |\psi_\beta'\rangle$ (7/2, 5/2) match the ^{1}H resonance frequency correspond to the positions of ^{1}H relaxation maxima denoted as II, III and V, respectively.

^{1}H single-quantum transition, while the origin of two others remain unexplained at this stage.

In Fig. 5(b) we compare this finding with the ^{1}H spin–lattice relaxation data for tris(2,6-dimethoxyphenyl)bismuthane. Again the QRE peaks II, III and V can be attributed to the ^{209}Bi transitions: $|\psi_\alpha\rangle \rightarrow |\psi_\alpha'\rangle$ (3/2, 1/2), $|\psi_\beta\rangle \rightarrow |\psi_\beta'\rangle$ (5/2, 3/2) and $|\psi_\gamma\rangle \rightarrow |\psi_\gamma'\rangle$ (7/2, 5/2), respectively, in analogy to tris-(2-methoxyphenyl)bismuthane, combined with a single quantum transition of ^{1}H. Analogously to tris(2-methoxyphenyl)bismuthane, peak IV cannot be attributed to a $|\psi_i\rangle \rightarrow |\psi_j\rangle$ (m_S, $m_S - 1$) transition (coherence). As far as the low frequency range is concerned, we restrain ourselves at this moment from numbering the QRE peaks, as for tris(2,6-dimethoxyphenyl)bismuthane they are less pronounced than for tris(2-methoxyphenyl)bismuthane.

The analysis clearly shows that the full QRE patterns of the investigated compounds cannot be fully explained in terms of the single quantum ^{1}H transition combined with one of the $|\psi_i\rangle \rightarrow |\psi_j\rangle$ (m_S, $m_S - 1$) ^{209}Bi transitions. However, as explained in Section 2, QRE effects can involve two coupled spin 1/2 nuclei. Therefore, in the next step we shall consider a combination of the double quantum ^{1}H transition with $|\psi_i\rangle \rightarrow |\psi_j\rangle$ (m_S, $m_S - 1$) ^{209}Bi transitions – such a scenario can take place in a system composed of one ^{209}Bi nucleus and two ^{1}H nuclei. In Fig. 6(a) (top) the frequency ranges are plotted in which the transition frequency of the ^{1}H double quantum transitions (twice the resonance frequency, 2ω) crosses one of the $|\psi_i\rangle \rightarrow |\psi_j\rangle$ (m_S, $m_S - 1$) ^{209}Bi transitions. Projecting these ranges onto the ^{1}H relaxation data for tris(2-methoxyphenyl)bismuthane reveals that the joint transition of two ^{1}H spins only contribute to QRE peak II – the origin of peaks I and IV still remain unexplained. Analogous analysis has been performed for tris(2,6-dimethoxyphenyl)bismuthane [Fig. 6(b)]. In this case the asymmetry of the quadrupole interaction ($\eta \neq 0$) affects the ^{209}Bi energy level structure and, in consequence, leads to a shift of the transition frequency $|\psi_\beta\rangle \rightarrow |\psi_\beta'\rangle$ (5/2, 3/2) which now yields a peak denoted as III^a instead of peak II like for $\eta = 0$. The notation reflects the fact that this QRE peak is a ^{1}H double quantum counterpart of peak III. This comparison between the cases of $\eta = 0$ and $\eta \neq 0$ implies that for $\eta = 0$ peak III^a overlaps with peak II. Including the possibility of joint single quantum transitions of two coupled ^{1}H nuclei (*i.e.* the double quantum transition) gives a better understanding of the QRE effects, but it still does not fully explain the QRE pattern.

Therefore we consider, in the next step, $|\psi_i\rangle \rightarrow |\psi_j\rangle$ (m_S, $m_S - 2$) transitions of ^{209}Bi combined with single quantum and double quantum ^{1}H transitions. Fig. 7(a) (top) shows $|\psi_i\rangle \rightarrow |\psi_j\rangle$ (m_S, $m_S - 2$) ^{209}Bi transition frequencies for tris(2-methoxyphenyl)-bismuthane and single and double quantum transition frequencies of ^{1}H. Following the same approach as above, the ranges in which the ^{209}Bi and ^{1}H transition frequencies match are projected onto the ^{1}H spin–lattice relaxation data. The first observation is that the range in which the $|\psi_i\rangle \rightarrow |\psi_j\rangle$ (m_S, $m_S - 2$) ^{209}Bi transition frequencies cross the ^{1}H resonance frequency is very broad and, in consequence, somewhat contributes to the "background" relaxation, but does not lead to distinct relaxation maxima. At the same time the $|\psi_i\rangle \rightarrow |\psi_j\rangle$ (m_S, $m_S - 2$) transition

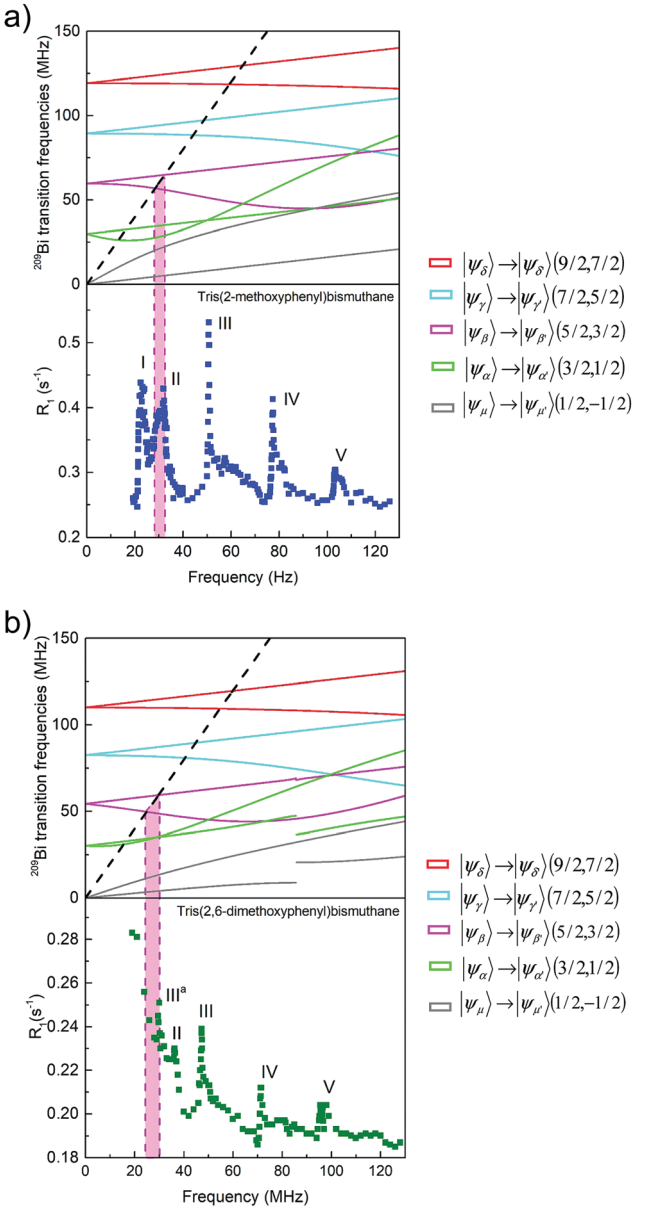

Fig. 6 (a). ^{209}Bi transition frequencies $|\psi_i\rangle \rightarrow |\psi_j\rangle$ (m_S, $m_S - 1$) in tris-(2-methoxyphenyl)bismuthane and twice ^{1}H resonance frequency (corresponding to ^{1}H double quantum transition) for the whole range of Ω angle, compared with the experimental ^{1}H spin–lattice relaxation data. The range in which the transition frequency $|\psi_\beta\rangle \rightarrow |\psi_\beta'\rangle$ (5/2, 3/2) matches the ^{1}H resonance frequency correspond to the positions of ^{1}H relaxation maxima denoted as II. (b) ^{209}Bi transition frequencies $|\psi_i\rangle \rightarrow |\psi_j\rangle$ (m_S, $m_S - 1$) in tris(2,6-methoxyphenyl)bismuthane and twice ^{1}H resonance frequency (corresponding to ^{1}H double quantum transition) for the whole range of Ω angle, compared with the experimental ^{1}H spin–lattice relaxation data. The range in which the transition frequency $|\psi_\beta\rangle \rightarrow |\psi_\beta'\rangle$ (5/2, 3/2) matches the ^{1}H resonance frequency correspond to the positions of ^{1}H relaxation maxima denoted as III^a.

frequencies compared with the frequency of 2ω lead to interesting results. The frequency of $|\psi_\delta\rangle \rightarrow |\psi_\gamma'\rangle$ (9/2, 5/2) ^{209}Bi transition covers the frequency range in which peak V is present. Nevertheless, taking into account probability of a double quantum ^{1}H transition is lower than of single quantum

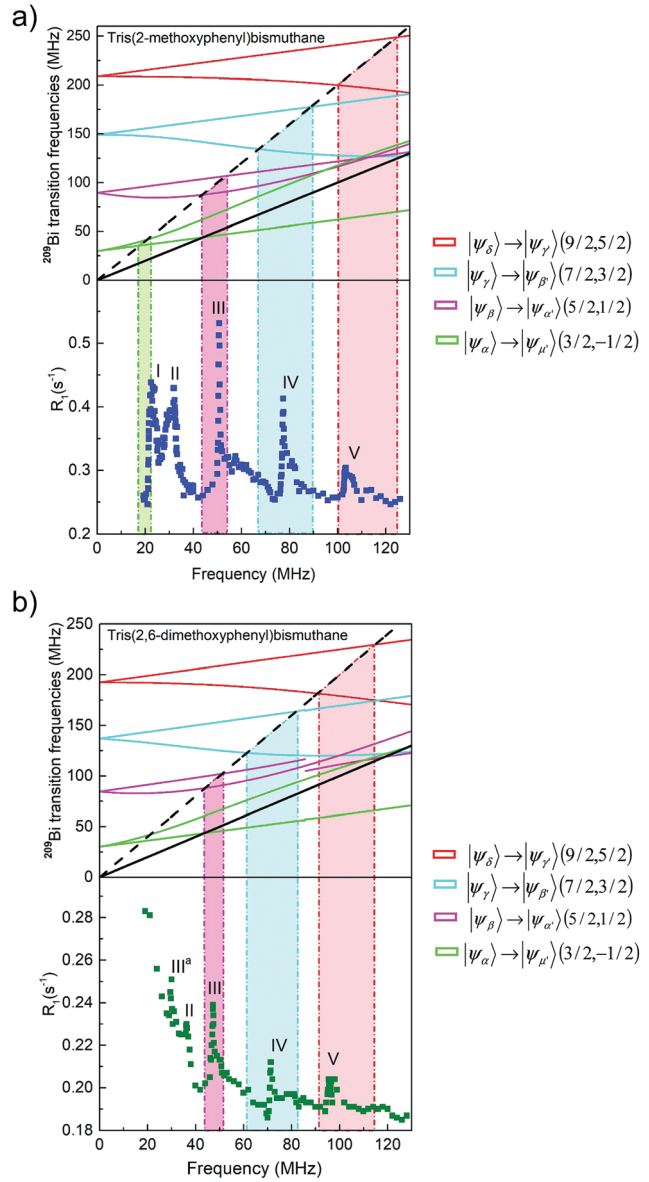

Fig. 7 (a) ^{209}Bi transition frequencies $|\psi_i\rangle \rightarrow |\psi_j\rangle$ (m_S, $m_S - 2$) in tris-(2-methoxyphenyl)bismuthane and ^{1}H resonance frequency and twice ^{1}H resonance frequency (corresponding to ^{1}H single and double quantum transitions, respectively) for the whole range of Ω angle compared with the experimental ^{1}H spin–lattice relaxation data. The ranges in which the transition frequencies $|\psi_\alpha\rangle \rightarrow |\psi_\mu'\rangle$ (3/2, −1/2), $|\psi_\beta\rangle \rightarrow |\psi_\alpha'\rangle$ (5/2, 1/2), $|\psi_\gamma\rangle \rightarrow |\psi_\beta'\rangle$ (7/2, 3/2) and $|\psi_\delta\rangle \rightarrow |\psi_\gamma'\rangle$ (9/2, 5/2) match the doubled ^{1}H resonance frequency correspond to the positions of ^{1}H relaxation maxima denoted as I, III, IV and V, respectively. (b) ^{209}Bi transition frequencies $|\psi_i\rangle \rightarrow |\psi_j\rangle$ (m_S, $m_S - 2$) in tris(2,6-dimethoxyphenyl)-bismuthane and ^{1}H resonance frequency and twice ^{1}H resonance frequency for the whole range of Ω angle compared with the experimental ^{1}H spin–lattice relaxation data. The ranges in which the transition frequencies $|\psi_\beta\rangle \rightarrow |\psi_\alpha'\rangle$ (5/2, 1/2), $|\psi_\gamma\rangle \rightarrow |\psi_\beta'\rangle$ (7/2, 3/2) and $|\psi_\delta\rangle \rightarrow |\psi_\gamma'\rangle$ (9/2, 5/2) match the doubled ^{1}H resonance frequency correspond to the positions of ^{1}H relaxation maxima denoted as III, IV and V, respectively.

ones and that the position of peak V has already been attributed to the $|\psi_\gamma\rangle \rightarrow |\psi_\gamma'\rangle$ (7/2, 5/2) ^{209}Bi transition combined with the ^{1}H resonance frequency, ω, one can expect that the contribution of the last one to the creation of peak V is more significant. Then the presence of peak IV can be attributed to the $|\psi_\gamma\rangle \rightarrow |\psi_\beta'\rangle$ (7/2, 3/2) ^{209}Bi transition combined with the ^{1}H double quantum transition, 2ω. Proceeding further, the $|\psi_\beta\rangle \rightarrow |\psi_\alpha'\rangle$ (5/2, 1/2) transition contributes to the formation of peak III (already associated with the $|\psi_\beta\rangle \rightarrow |\psi_\alpha'\rangle$ (5/2, 1/2) transition combined with ^{1}H single quantum transition). Then again, the so far unexplained presence of peak I can be attributed to the $|\psi_\alpha\rangle \rightarrow |\psi_\mu'\rangle$ (3/2, −1/2) ^{209}Bi transition combined with ^{1}H double quantum transition. Analogous pattern has been found for tris(2,6-dimethoxyphenyl)bismuthane [Fig. 7(b)]. Here also the $|\psi_\delta\rangle \rightarrow |\psi_\gamma'\rangle$ (9/2, 5/2) and $|\psi_\beta\rangle \rightarrow |\psi_\alpha'\rangle$ (5/2, 1/2) ^{209}Bi transitions combined with double quantum ^{1}H transition can give a contribution to the QRE effects reflected by peak V and peak III, respectively, while the position of peak IV corresponds to the range in which the frequency of $|\psi_\gamma\rangle \rightarrow |\psi_\beta'\rangle$ (7/2, 3/2) transition matches the frequency of double quantum ^{1}H transition. On the basis of the experimental data for tris(2,6-dimethoxyphenyl)-bismuthane ($C_{24}H_{27}BiO_6$) one can hardly discuss the possibility of the presence of a counterpart of peak I observed for tris-(2-methoxyphenyl)bismuthane.

5. Conclusions

In order to reveal the quantum-mechanical picture of QRE effects for ^{209}Bi in the context of a novel mechanism of MRI contrast, NQR and NMR relaxometry studies have been performed for tris(2-methoxyphenyl)bismuthane and tris(2,6-dimethoxyphenyl)bismuthane in powder. On the basis of the NQR spectra the quadrupole parameters for both compounds have been determined: a_Q = 715.27 MHz, η = 0 for tris-(2-methoxyphenyl)bismuthane and a_Q = 660.94 MHz, η = 0.105 for tris(2,6-dimethoxyphenyl)bismuthane. On the basis of these parameters the ^{1}H spin–lattice QRE patterns, collected in the magnetic field range of 0.5 T–3 T, have been attributed to specific spin transitions. In the first step $|\psi_i\rangle \rightarrow |\psi_j\rangle$ (m_S, $m_S - 1$) ^{209}Bi transitions combined with ^{1}H single quantum transition have been considered. It has been shown that this combination explains the existence of three ^{1}H spin–lattice relaxation maxima observed at the ^{1}H frequency of 27–36 MHz (peak II), 50–71 MHz (peak III) and 85–107 MHz (peak V) for tris-(2-methoxyphenyl)bismuthane and of 35–42 MHz (peak II), 46–65 MHz (peak III) and 76–98 MHz (peak V) for tris(2,6-dimethoxyphenyl)bismuthane, corresponding to the $|\psi_\alpha\rangle \rightarrow |\psi_\alpha'\rangle$ (3/2, 1/2), $|\psi_\beta\rangle \rightarrow |\psi_\beta'\rangle$ (5/2, 3/2) and $|\psi_\gamma\rangle \rightarrow |\psi_\gamma'\rangle$ (7/2, 5/2) ^{209}Bi transitions. Joint ^{1}H double-quantum transition combined with the $|\psi_\beta\rangle \rightarrow |\psi_\beta'\rangle$ (5/2, 3/2) ^{209}Bi transition for tris(2,6-dimethoxyphenyl)bismuthane gives rise to the quadrupole peak observed at 24–30 MHz (peak III^a) (it is a double quantum counterpart of the maximum observed at 46–65 MHz (peak III)); for tris(2-methoxyphenyl)bismuthane this combination leads to a QRE effect which overlaps with the peak originating from ^{1}H single quantum transition combined with the $|\psi_\beta\rangle \rightarrow |\psi_\beta'\rangle$ (3/2, 1/2) ^{209}Bi transition. The peaks observed at the ^{1}H frequency of 99–125 MHz (peak V), 66–89 MHz

(peak IV) and 43–54 MHz (peak III) for tris(2-methoxyphenyl)-bismuthane and of 91–114 MHz (peak V), 61–82 MHz (peak IV) and 44–52 MHz (peak III) for tris(2,6-dimethoxyphenyl)-bismuthane can include contributions originating from combinations of ^{1}H double quantum transitions with ^{209}Bi $|\psi_i\rangle \rightarrow |\psi_j\rangle$ (m_S, $m_S - 2$) transitions: $|\psi_\delta\rangle \rightarrow |\psi_\gamma'\rangle$ (9/2, 5/2), $|\psi_\delta\rangle \rightarrow |\psi_\gamma'\rangle$ (7/2, 3/2) and $|\psi_\beta\rangle \rightarrow |\psi_\alpha'\rangle$ (5/2, 1/2), respectively. Moreover, for tris(2-methoxyphenyl)bismuthane the combination of ^{1}H double quantum transition with the $|\psi_i\rangle \rightarrow |\psi_j\rangle$ (3/2, −1/2) transition explains the presence of the quadrupole peak at the frequency of 16–23 MHz (peak I).

This thorough analysis reveals the quantum-mechanical background of the observed QRE effects. This is, to our knowledge, a first example of QRE effects for high spin quantum numbers of a quadrupolar nucleus reported and discussed in the literature and demonstrates the existence of one important prerequisite for the potential use of the phenomenon for medical imaging.

Conflicts of interest

There are no conflicts to declare.

Appendix

Matrix elements of the Hamiltonian, $H_0(S)$ in the $\{|S,m_S\rangle\}$ basis take the form:

diagonal elements:

$$\left\langle \pm\frac{9}{2}\middle|H_0(S)\middle|\pm\frac{9}{2}\right\rangle = \pm\frac{9}{2}\omega_S + \frac{1}{16}a_Q\left[1+3\cos(2\beta)+2\eta\cos(2\alpha)\sin^2(\beta)\right]$$

$$\left\langle \pm\frac{7}{2}\middle|H_0(S)\middle|\pm\frac{7}{2}\right\rangle = \pm\frac{7}{2}\omega_S + \frac{1}{48}a_Q\left[1+3\cos(2\beta)+2\eta\cos(2\alpha)\sin^2(\beta)\right]$$

$$\left\langle \pm\frac{5}{2}\middle|H_0(S)\middle|\pm\frac{5}{2}\right\rangle = \pm\frac{5}{2}\omega_S - \frac{1}{96}a_Q\left[1+3\cos(2\beta)+2\eta\cos(2\alpha)\sin^2(\beta)\right]$$

$$\left\langle \pm\frac{3}{2}\middle|H_0(S)\middle|\pm\frac{3}{2}\right\rangle = \pm\frac{3}{2}\omega_S - \frac{1}{32}a_Q\left[1+3\cos(2\beta)+2\eta\cos(2\alpha)\sin^2(\beta)\right]$$

$$\left\langle \pm\frac{1}{2}\middle|H_0(S)\middle|\pm\frac{1}{2}\right\rangle = \pm\frac{1}{2}\omega_S - \frac{1}{24}a_Q\left[1+3\cos(2\beta)+2\eta\cos(2\alpha)\sin^2(\beta)\right]$$

off diagonal elements:

$$\left\langle \frac{9}{2}\middle|H_0(S)\middle|\frac{7}{2}\right\rangle = -\left\langle -\frac{7}{2}\middle|H_0(S)\middle|-\frac{9}{2}\right\rangle = \frac{1}{12}a_Q e^{i\gamma}\{[-3+\eta\cos(2\alpha)]\cos(\beta) + i\eta\sin(2\alpha)\}\sin(\beta),$$

$$\left\langle \frac{7}{2}\middle|H_0(S)\middle|\frac{5}{2}\right\rangle = -\left\langle -\frac{5}{2}\middle|H_0(S)\middle|-\frac{7}{2}\right\rangle = \frac{1}{12}a_Q e^{i\gamma}\{[-3+\eta\cos(2\alpha)]\cos(\beta) + i\eta\sin(2\alpha)\}\sin(\beta),$$

$$\left\langle \frac{5}{2}\middle|H_0(S)\middle|\frac{3}{2}\right\rangle = -\left\langle -\frac{3}{2}\middle|H_0(S)\middle|-\frac{5}{2}\right\rangle = \frac{1}{24}\sqrt{\frac{7}{3}}a_Q e^{i\gamma}\{[-3+\eta\cos(2\alpha)]\cos(\beta) + i\eta\sin(2\alpha)\}\sin(\beta),$$

$$\left\langle \frac{3}{2}\middle|H_0(S)\middle|\frac{1}{2}\right\rangle = -\left\langle -\frac{1}{2}\middle|H_0(S)\middle|-\frac{3}{2}\right\rangle = \frac{1}{12\sqrt{6}}a_Q e^{i\gamma}\{[-3+\eta\cos(2\alpha)]\cos(\beta) + i\eta\sin(2\alpha)\}\sin(\beta),$$

$$\left\langle \frac{9}{2}\middle|H_0(S)\middle|\frac{5}{2}\right\rangle = \left\langle -\frac{5}{2}\middle|H_0(S)\middle|-\frac{9}{2}\right\rangle = \frac{1}{48}a_Q e^{-2i(\alpha-\gamma)}\left[2e^{4i\alpha}\eta\cos^4\left(\frac{\beta}{2}\right)+2\eta\sin^4\left(\frac{\beta}{2}\right) + 3e^{2i\alpha}\sin^2(\beta)\right]$$

$$\left\langle \frac{7}{2}\middle|H_0(S)\middle|\frac{3}{2}\right\rangle = \left\langle -\frac{3}{2}\middle|H_0(S)\middle|-\frac{7}{2}\right\rangle = \frac{1}{48}\sqrt{\frac{7}{3}}a_Q e^{-2i(\alpha-\gamma)}\left[2e^{4i\alpha}\eta\cos^4\left(\frac{\beta}{2}\right)+2\eta\sin^4\left(\frac{\beta}{2}\right) + 3e^{2i\alpha}\sin^2(\beta)\right]$$

$$\left\langle \frac{5}{2}\middle|H_0(S)\middle|\frac{1}{2}\right\rangle = \left\langle -\frac{1}{2}\middle|H_0(S)\middle|-\frac{5}{2}\right\rangle = \frac{1}{48}\sqrt{\frac{7}{2}}a_Q e^{-2i(\alpha-\gamma)}\left[2e^{4i\alpha}\eta\cos^4\left(\frac{\beta}{2}\right)+2\eta\sin^4\left(\frac{\beta}{2}\right) + 3e^{2i\alpha}\sin^2(\beta)\right]$$

$$\left\langle \frac{3}{2}\middle|H_0(S)\middle|-\frac{1}{2}\right\rangle = \left\langle \frac{1}{2}\middle|H_0(S)\middle|-\frac{3}{2}\right\rangle = \frac{5}{48\sqrt{6}}a_Q e^{-2i(\alpha-\gamma)}\left[2e^{4i\alpha}\eta\cos^4\left(\frac{\beta}{2}\right)+2\eta\sin^4\left(\frac{\beta}{2}\right) + 3e^{2i\alpha}\sin^2(\beta)\right]$$

The elements of the $H_0(S)$ matrix below the diagonal are given as $\langle m|H_0(S)|n\rangle = \langle n|H_0(S)|m\rangle^*$, where "*"denotes complex conjugation. Other elements are equal to zero.

Acknowledgements

This project has received funding from the European Union's Horizon 2020 research and innovation programme under grant agreement no. 665172.

References

1 R. Damadian, *Science*, 1971, **171**, 1151.
2 I. C. Kiricuta and V. Simplăceanu, *Cancer Res.*, 1975, **35**, 1164.
3 J. Kowalewski, D. Kruk and G. Parigi, *Adv. Inorg. Chem.*, 2005, **57**, 41.
4 E. Belorizky, P. H. Fries, L. Helm, J. Kowalewski, D. Kruk, R. R. Sharp and P.-O. Westlund, *J. Chem. Phys.*, 2008, **128**, 052315.
5 P. Caravan, *Chem. Soc. Rev.*, 2006, **35**, 512.
6 D. Kruk, T. Nilsson and J. Kowalewski, *Phys. Chem. Chem. Phys.*, 2001, **3**, 4907.
7 D. Kruk and J. Kowalewski, *Mol. Phys.*, 2003, **101**, 2861.
8 I. Bertini, O. Galas, C. Luchinat and G. Parigi, *J. Magn. Reson.*, 1995, **113**, 151.
9 T. Nilsson, J. Svoboda, P.-O. Westlund and J. Kowalewski, *J. Chem. Phys.*, 1998, **109**, 6364.
10 P. Caravan, J. J. Ellison, T. J. McMurry and R. B. Lauffer, *Chem. Rev.*, 1999, **99**, 2293.
11 É. Tóth, L. Helm and A. E. Merbach, *Contrast Agents I*, ed. W. Krause, Springer-Verlag, Germany, 2002, p. 61.
12 I. Solomon and N. Bloembergen, *J. Chem. Phys.*, 1956, **25**, 261.
13 N. Bloembergen and L. O. Morgan, *J. Chem. Phys.*, 1961, **34**, 842.
14 P.-O. Westlund, *J. Chem. Phys.*, 1998, **108**, 4945.
15 D. Kruk, J. Kowalewski, D. S. Tipikin, J. H. Freed, M. Mościcki, A. Mielczarek and M. Port, *J. Chem. Phys.*, 2011, **134**, 024508.
16 D. Kruk and J. Kowalewski, *J. Chem. Phys.*, 2009, **130**, 174104.
17 S. Laurent, D. Forge, M. Port, A. Roch, C. Robic, L. V. Elst and R. N. Muller, *Chem. Rev.*, 2008, **108**, 2064.
18 D. Kruk, A. Korpała, S. M. Taheri, A. Kozłowski, S. Förster and E. A. Rössler, *J. Chem. Phys.*, 2014, **140**, 174504.
19 D. V. Hingorani, A. S. Bernstein and M. D. Pagel, *Contrast Media Mol. Imaging*, 2015, **10**, 245.
20 F. Winter and R. Kimmich, *Mol. Phys.*, 1982, **45**, 33.
21 F. Winter and R. Kimmich, *Biophys. J.*, 1985, **48**, 331.
22 E. Anoardo and D. J. Pusiol, *Phys. Rev. Lett.*, 1996, **76**, 3983.
23 E. P. Sunde and B. Halle, *J. Magn. Reson.*, 2010, **203**, 257.
24 L. M. Broche, G. P. Ashcroft and D. J. Lurie, *Magn. Reson. Med.*, 2012, **68**, 358.
25 P.-O. Westlund, *Phys. Chem. Chem. Phys.*, 2010, **12**, 3136.
26 M. Florek-Wojciechowska, M. Wojciechowski, R. Jakubas, S. Brym and D. Kruk, *J. Chem. Phys.*, 2016, **144**, 054501.
27 M. Florek-Wojciechowska, R. Jakubas and D. Kruk, *Phys. Chem. Chem. Phys.*, 2017, **19**, 11197.
28 D. Kruk, A. Kubica, W. Masierak, A. F. Privalov, M. Wojciechowski and W. Medycki, *Solid State Nucl. Magn. Reson.*, 2011, **40**, 114.
29 M. Nolte, A. Privalov, J. Altmann, V. Anferov and F. Fujara, *J. Phys. D: Appl. Phys.*, 2002, **35**, 939.
30 D. Kruk, J. Altmann, F. Fujara, A. Gädke, M. Nolte and A. F. Privalov, *J. Phys.: Condens. Matter*, 2005, **17**, 519.
31 D. Kruk and O. Lips, *Solid State Nucl. Magn. Reson.*, 2005, **28**, 180.
32 D. Kruk and O. Lips, *J. Magn. Reson.*, 2006, **179**, 250.
33 D. Kruk, *Understanding Spin Dynamics*, Pan Stanford Publishing Pte. Ltd., Singapore, 2016.
34 D. M. Brink and G. R. Satchler, *Angular Momentum*, Clarendon Press, Oxford, 1979.
35 A. R. Edmonds, *Angular Momentum in Quantum Mechanics*, Princeton University Press, Princeton, 1974.
36 H. Scharfetter, *J. Magn. Reson.*, 2016, **271**, 90.